Contrasting responses of autumn leaf senescence to daytime and nighttime warming

Chaoyang Wu[1,2*], Xiaoyue Wang[1,2], Huanjiong Wang[1,2*], Philippe Ciais[3], Josep Peñuelas[4,5], Ranga B. Myneni[6], Ankur R. Desai[7], Christopher M. Gough[8], Alemu Gonsamo[9], Andrew T. Black[10,] Rachhpal S. Jassal[10], Weimin Ju[11], Wenping Yuan[12], Yongshuo Fu[13], Miaogen Shen[14], Shihua Li[15], Ronggao Liu[16], Jing M. Chen[9], Quansheng Ge[1, 2]*

1. The Key Laboratory of Land Surface Pattern and Simulation, Institute of Geographical Sciences and Natural Resources Research, Chinese Academy of Sciences, Beijing 100101, China;
2. University of the Chinese Academy of Sciences, Beijing 100049, China;
3. Laboratoire des Sciences du Climat et de l'Environnement, IPSL-LSCE CEA CNRS UVSQ, 91191, Gif sur, Yvette, France;
4. CSIC, Global Ecology Unit CREAF-CSIC-UAB, Bellaterra, Barcelona 08193, Catalonia, Spain.
5. CREAF, Cerdanyola del Valles, Barcelona 08193, Catalonia, Spain;
6. Department of Earth and Environment, Boston University, 685 Commonwealth Avenue, Boston, MA 02215, USA;
7. Department of Atmospheric and Oceanic Sciences, University of Wisconsin-Madison, Madison, WI, USA;
8. Department of Biology, Virginia Commonwealth University, Richmond, VA 23284-2012, USA;
9. Department of Geography and Planning, University of Toronto, 100 St. George St., Toronto, ON, M5S 3G3, Canada;
10. Faculty of Land and Food Systems, University of British Columbia, Vancouver, BC, Canada;
11. International Institute for Earth System Science, Nanjing University, 22 Hankou Road, Nanjing, 210093, China;
12. School of Atmospheric Sciences, Center for Monsoon and Environment Research, Sun Yat-Sen University, Guangzhou 510275, China;
13. College of Water Sciences, Beijing Normal University,100875, Beijing, China;
14. CAS Center for Excellence in Tibetan Plateau Earth Sciences, Beijing 100101, China;
15. School of Resources and Environment, University of Electronic Science and Technology of China, Chengdu 611731, China;
16. State key Laboratory of Resources and Environmental Information system, Institute of Geographic Sciences and Natural Resources Research, CAS, Beijing 100101, China

***Corresponding authors:** C Wu (wucy@igsnrr.ac.cn), H Wang (wanghj@igsnrr.ac.cn) and Q Ge (geqs@igsnrr.ac.cn).

Plant phenology is a sensitive indicator of climate change[1-4], and plays a significant role in regulating carbon uptake by plants[5-7]. Previous studies have focused on spring leaf-out by daytime temperature and the onset of snowmelt time[8-9], but the drivers controlling leaf senescence date (LSD) in autumn remain largely unknown[10-12]. Using long-term ground phenological records (14536 time series since the 1900s) and satellite greenness observations dating back to the 1980s, we show that rising preseason maximum daytime (T_{day}) and minimum nighttime (T_{night}) temperatures had contrasting effects on the timing of autumn LSD in the Northern Hemisphere (>20°N). If higher T_{day} leads to an earlier or later LSD, an increase in T_{night} systematically drives LSD to occur oppositely. Contrasting impacts of daytime and nighttime warming on drought stress may be the underlying mechanism. A new LSD model considering these opposite effects improved autumn phenology modeling, and predicted an overall earlier autumn LSD by the end of this century compared with traditional projections. These results challenge the notion of prolonged growth under higher autumn temperatures, suggesting instead that leaf senescence in the Northern Hemisphere will begin earlier than currently expected, causing a positive climate feedback.

Climate change over the last several decades has modified the dates of plant flowering, leaf emergence, growth stages, and senescence, collectively termed phenology[13] with substantial ecological and environmental consequences[4]. Both observations and model simulations have found that air temperature has a positive influence on the onset of plant growth in the Northern Hemisphere (NH), e.g., higher spring temperature triggers earlier

leaf-out and flowering dates and hence extends the growing season[8,14-15]. In contrast to those extensive research efforts on spring phenology, autumn phenology, particularly leaf senescence date (LSD), is more challenging to understand, and has not received sufficient attention[16,17], while also serving as an important indicator of changing foliar physiological properties. Yet, autumn phenology may be as important as spring in regulating the interannual variability of carbon balance[7].

LSD has been occurring later in most regions over the last few decades[18], but providing an explanation for this change is difficult[9]. An increase in global temperature is assumed to be a driver of LSD trends[19], but studies indicated that the contribution of temperature to LSD variability is low, especially compared to spring phenology[20,21]. We argue that ignoring the asymmetric effects[22] of daytime maximum temperature (T_{day}) versus nighttime minimum temperature (T_{night}) and their differing impacts on LSD, contributes to the reported overall low contribution of temperature to LSD variability. To test this, we used measured and gridded preseason (defined as months from June to LSD) T_{day} and T_{night} in the NH, together with LSD data from three different datasets: (a) long-term phenological observations at ground sites from 14536 time series since the 1900s (Fig. S1), (b) the latest third generation of the Normalized Difference Vegetation Index (NDVI, GIMMS3g.v1) for 1982-2015, and (c) NDVI and enhanced vegetation index (EVI) from the Moderate Resolution Imaging Spectroradiometer (MODIS) products for 2001-2015.

Preseason forcing had a better predictive strength on LSD than either summer or autumn

84 climate forcing alone (Fig. S2). Because preseason T_{day} and T_{night} were highly correlated,
85 we used a partial correlation to remove the effects of T_{night} and of precipitation and
86 radiation (similarly for T_{night}) to investigate the response of LSD to T_{day}. Correlations were
87 classified into four types, (A) $T_{day}^{+}T_{night}^{+}$, (B) $T_{day}^{-}T_{night}^{-}$, (C) $T_{day}^{+}T_{night}^{-}$ and (D) $T_{day}^{-}T_{night}^{+}$,
88 where T^{+}, T^{-} represent positive and negative partial correlation coefficient of T with LSD.
89
90 Overall, all three datasets suggested that the onset of autumn LSD responded oppositely
91 to T_{day} and T_{night}. The proportions of ground sites of Types A and B were significantly lower
92 than those of Type C and D (Fig. 1a). More significant R values for both T_{day} and T_{night}
93 were found within Types C and D, with only two and one records out of 2231 time series
94 having significant R within Type A and B, respectively. These results from ground sites
95 are consistent with those for the two satellite greenness products (Fig. 1b, c). Types C and
96 D together accounted for 83.7 and 80.0% for GIMMS3g and MODIS pixels, respectively.
97 Only 0.8 and 1.5% of the pixels had the same sign of response of LSD to T_{day} or T_{night} (i.e.
98 significant pixels for Types A+B) for GIMMS3g and MODIS, respectively. The GIMMS3g
99 dataset contained different fractions of Types C and D (45.6% vs. 38.1%), but the
100 compositions of Type C and D in GIMMS3g (i.e., contrasting effects of night and day
101 temperatures) became more consistent with the MODIS results when the overlapping
102 periods between the two sensors is considered (Figs. S3-4). More details on the fractions
103 of the four correlation types for different vegetation types are provided in Figs. S5-6.
104
105 **Figure 1 Frequency of the partial correlation coefficient (R) between leaf senescence date**

(LSD) and daytime (T_{day}), nighttime (T_{night}) temperatures. (a) Data for 14536 time series of ground sites, (b) the GIMMS3g dataset for 1982-2015, and (c) the MODIS product for 2001-2015. T^+, T^- represent positive and negative partial correlation coefficient of T with LSD. Significance was set at $P < 0.05$.

The satellite greenness products also allowed us to evaluate spatial patterns of LSD changes in response to variations in T_{day} and T_{night} (Fig. 2). For the GIMMS3g data, higher T_{day} was associated with a delayed LSD for 10.7% of the pixels (mostly boreal regions) and with an earlier LSD for 7.5% of the pixels (central North America, borders of Eurasia and central China). T_{night} had evident opposite influences on LSD than T_{day}. The patterns of opposite effects from T_{day} and T_{night} on LSD were highly spatially consistent in all regions where T_{day} and T_{night} were significantly correlated with LSD. Similar results were obtained with MODIS observations (Fig. 2b, d). LSD for approximately 20% all pixels was significantly correlated with T_{day}, of which 60.1 and 39.9% were negatively and positively correlated, respectively. The area where LSD was positively correlated with T_{night} was larger (9.4%) than the area with negative correlations (6.5%).

Vegetation grouped into Köppen-Geiger zones showed contrasting patterns between the effects of T_{day} and T_{night} on LSD (Fig. 2e, f). Type D was more widely distributed, while Type C was more common for continental climates. Monsoon-influenced but not extremely cold regions and mild climates also had higher proportions of Type C. Grouping these correlation types by vegetation types lead to similar results (Fig. 2g, h). In theory,

we would expect to find Type C more in wet vegetation types and Type D in dry types. The real world seems to show the same thing but still there could be many locations that do not neatly fall into that continuum and suggests additional mechanisms may work, probably adaption.

Figure 2 Spatial distributions of the partial correlation coefficient (R) between leaf senescence date (LSD) and daytime (T_{day}), nighttime (T_{night}) temperatures. R^+, R^- represent positive and negative partial correlation coefficient of T with LSD. (a) LSD vs. T_{day} for GIMMS3g, (b) LSD vs. T_{day} for MODIS, (c) LSD vs. T_{night} for GIMMS3g, and (d) LSD vs. T_{night} for MODIS. (e), (f), represent distributions of correlation types in Köppen-Geiger climatic classification using GIMMS3g and MODIS, respectively. (g) and (h) represent distributions of correlation types for vegetation types (see Methods) using GIMMS3g and MODIS, respectively. Significance was set at $P < 0.05$.

Our results suggest that ecological trade-offs, particularly those driven by regional differences in water stress, may underlie the contrasting relationships between LSD and T_{day} and T_{night}. Type C was mostly found in humid regions where water is a less limiting factor for plant growth. In these cases, a higher T_{day}, in the likely absence of severe water stress, benefits photosynthesis while elevated T_{night} increases nighttime leaf respiration.

Explanations for the prevalence of Type D relations in dry regions are more complicated. The Standardized Precipitation Evapotranspiration Index (SPEI)[23], an indicator of drought

150 stress, accounted for the contrasting effects of increases in T_{day} and T_{night} on LSD for Type
151 D (Fig. 3). Partial correlation data indicate that increased T_{day} is negatively correlated with
152 SPEI (Fig. 3a), a stronger sensitivity to drought in dry regions that negatively affects plant
153 growth and consequently leads to an earlier LSD. In contrast, we found that an increase in
154 T_{night} is associated with a higher SPEI, that is, wetter conditions, and arguably reduced
155 water stress, which could extend the duration of photosynthesisand lead to delayed LSD
156 (Fig. 3b). The latter mechanism is consistent with the generally positive partial correlation
157 values between evapotranspiration (ET) and T_{night}, that is, more soil moisture being
158 available for ET in the lateseason, and sustaining delayed LSD (Fig. 3f), and with studies
159 showing that water stress accelerates leaf drop in dry ecosystems more so than in humid
160 ecosystems[24]. The responses of radiation to T_{day} and T_{night} may also be viewed as a
161 further evidence for the linkage between leaf senescence and plant water status to
162 support the contrasting patterns (Fig. S7), given that a higher T_{day} was associated with
163 stronger radiation and potentially a higher chance of water stress. These findings suggest
164 that dry regions, in which Type D dominates, may be especially vulnerable to earlier onset
165 of LSD if climate change reduces local precipitation and increases daytime evaporation
166 with rising T_{day}.
167
168 Apart from physiological mechanisms relating to water stress, ecological processes may
169 also contribute to these patterns. Warmer daytime versus nighttime temperature may
170 have contrasting effects on different species since species adaptations lead to intrinsic
171 differences in their timing of leaf emergence and senescence that are optimized to

maximize carbon gain and minimize water losses[25-27]. The ecosystem-scale responses of phenology reflects the scaled responses of ecological dynamics of multiple individual species gaining or losing a competitive advantage in a changing climate, or presenting an induced advantage as a result of land-use change and planting[17,26]. Recent results suggest that the magnitude of phenological change to effects by shifts in plant species composition may be similar as that by climate change[27], and the autumn phenology may thus change accordingly.

Figure 3 Partial correlation coefficient (R) between the Standardized Precipitation Evapotranspiration Index (SPEI), evapotranspiration (ET), and daytime (T_{day}), nighttime (T_{night}) temperatures. (a) SPEI vs. T_{day} for GIMMS3g, (b) SPEI vs. T_{night} for GIMMS3g, (c) SPEI vs. T_{day} for MODIS, (d) SPEI vs. T_{night} for MODIS, (e) ET vs. T_{day} for MODIS, and (f) ET vs. T_{night} for MODIS. Significance was set at $P < 0.05$.

We tested the implications of the observation analysis on future trends in autumn LSD by developing a weighted day-night-temperature growing-degree-day (DN_{GDD}) algorithm incorporating these opposite changes in LSD to T_{day} and T_{night} (see Methods). The new model substantially improved LSD modeling (in terms of R (Figs. S8-10), RMSE (Figs. S11-13) and percentage of significant pixels (Figs. S14-15)) compared with the currently used threshold or GDD methods both for the overall dataset and for vegetation types.

Spatial patterns of improvements using MODIS and GIMMS3g were also investigated

(Figs. S16-17). The results from MODIS and the ground sites (Fig. S18) were more consistent with the new model, and the accuracy of the threshold method was much lower, so we used the coefficients from the MODIS data to predict LSD variability by the end of this century using traditional GDD and DN_{GDD} algorithms under two Representative Concentration Pathways (RCP) scenarios (RCP 4.5 and RCP 8.5) (Fig. S19, and Fig. 4).

LSD from the DN_{GDD} method was overall earlier than conventional predictions across Köppen-Geiger climatic classification types. Globally, LSD was earlier for about 68% of the terrestrial biosphere under RCP 4.5 and for about 70% under RCP 8.5. LSD was mostly later for central North America, western Russia, and southwestern China. Most vegetation types showed earlier LSD estimates under two RCP scenarios while the temperate grasslands were expected to have later senescence dates.

Figure 4 Leaf senescence date (LSD) differences from the weighted day-night-temperature growing-degree-day (DN_{GDD}) and traditional GDD (LSD_{DNGDD}-LSD_{GDD}) models under two RCP scenarios. (a), (b), (c) represent LSD_{DNGDD}-LSD_{GDD} under RCP 4.5, and averages of differences for the Köppen-Geiger climatic classification, and vegetation types, respectively. (d), (e), (f) represent LSD_{DNGDD}-LSD_{GDD} under RCP 8.5, and averages of differences for the Köppen-Geiger climatic classification, and vegetation types, respectively.

Climatic variability, particularly temperature, has driven phenological changes over the last several decades but has been challenging to predict. Our ability to predict autumn LSD is particularly limited. We are the first to report, using14536 ground time series and more than 30 years of remotely sensed observations, the opposite responses of LSD to daytime and nighttime warming, providing a new perspective to account for the previous low estimation accuracy of autumn LSD when relying solely on mean temperature. A model based on mean temperature cannot correctly predict LSD changes, because LSD responds to T_{day} and T_{night} in opposite directions. Our results also provide a perspective to account for the carry-over effects between spring and autumn phenology, i.e. the start and end of a growing season always move in the same direction[28]. An earlier start of a season is mainly triggered by higher spring temperatures, with increased growth depleting soil water[29], which is then associated with autumn drought, inducing a reduction in growth and consequently leading to an earlier end to the growing season[30].

Our improvement in modeling autumn phenology is a strong and convincing evidence for the value of incorporating daytime and nighttime temperatures in terrestrial models, rather than mean temperature alone. The application of this model projects an overall earlier than currently expected start of autumn senescence in the NH by the end of this century, particularly in dry regions. The earlier data of autumn senescence may be a potentially unrecognized positive feedback to climate change and consequently a weakening in the capability of terrestrial carbon uptake.

Acknowledgments: This work was funded by the Strategic Priority Research Program of the Chinese Academy of Sciences (XDA19040103), International Cooperation and Exchange Programs of National Science Foundation of China (Sino-German, 41761134082), National Natural Science Foundation of China (41522109) and the key Research Program of Frontier Sciences, CAS (QYZDB-SSW-DQC011). J.P. and P.C. were funded by European Research Council Synergy grant ERC-SyG-2013-610028 IMBALANCE-P. A.R.D. acknowledges support from the Ned P Smith Professorship of Climatology, University of Wisconsin-Madison.

Contributions: C.W., H.W. and Q.G. designed the research. C.W. wrote the first draft of the paper. J.P. and C.P. extensively revised the writing. H.W. performed the site model simulations. X.W. performed remote sensing model simulations. All the authors contributed to writing the paper.

Correspondence and requests for materials should be addressed C.W.

Competing interests: The authors declare no competing financial interests.

References

1. Fu, Y. H., et al (2015). Declining global warming effects on the phenology of spring leaf unfolding. Nature, 526, 104-107.

2. Xia, J., et al (2015). Joint control of terrestrial gross primary productivity by plant

phenology and physiology. Proceedings of the National Academy of Sciences, 112, 2788-2793.

3. Buitenwerf, R., et al (2015). Three decades of multi-dimensional change in global leaf phenology. Nature Climate Change, 5, 364.

4. Peñuelas, J., & Filella, I. (2009). Phenology feedbacks on climate change. Science, 324, 887-888.

5. Richardson, A. D., et al (2013). Climate change, phenology, and phenological control of vegetation feedbacks to the climate system. Agricultural and Forest Meteorology, 169, 156-173.

6. Keenan, T.F., et al. (2014) Net carbon uptake has increased through warming-induced changes in temperate forest phenology. Nature Climate Change, 4, 598-604.

7. Wu, C., et al (2013). Interannual variability of net ecosystem productivity in forests is explained by carbon flux phenology in autumn. Global Ecology and Biogeography, 22, 994-1006.

8. Piao, S., et al (2015). Leaf onset in the northern hemisphere triggered by daytime temperature. Nature communications, 6, doi:10.1038/ncomms7911.

9. Pulliainen, J., et al. (2017). Early snowmelt significantly enhances boreal springtime carbon uptake. Proceedings of the National Academy of Sciences, 114,11081-11086.

10. Liu, Q., et al. (2016). Delayed autumn phenology in the Northern Hemisphere is related to change in both climate and spring phenology. Global change biology, 22, 3702-3711.

11. Keenan, T.F., & Richardson, A. D. (2015). The timing of autumn senescence is

282 affected by the timing of spring phenology: implications for predictive models. Global
283 Change Biology, 21, 2634-2641.
284 12. Gill, A.L., et al (2015). Changes in autumn senescence in northern hemisphere
285 deciduous trees: a meta-analysis of autumn phenology studies. Annals of botany, 116,
286 875-888.
287 13. Myneni, R.B., et al (1997). Increased plant growth in the northern high latitudes from
288 1981 to 1991. Nature, 386, 698-702.
289 14. Suni, T., et al (2003). Air temperature triggers the recovery of evergreen boreal forest
290 photosynthesis in spring. Global Change Biology, 9, 1410–1426.
291 15. Richardson, A.D., et al (2012). Terrestrial biosphere models need better
292 representation of vegetation phenology: results from the North American Carbon Program
293 Site Synthesis. Global Change Biology, 18, 566-584.
294 16. Gallinat, A.S., et al (2015). Autumn, the neglected season in climate change
295 research. Trends in Ecology & Evolution, 30, 169-176.
296 17. Walther, G.R., et al (2002). Ecological responses to recent climate
297 change. Nature, 416, 389-395.
298 18. Zhu, W., et al (2012). Extension of the growing season due to delayed autumn over
299 mid and high latitudes in North America during 1982–2006. Global Ecology and
300 Biogeography, 21, 260-271.
301 19. Garonna, I., et al (2014). Strong contribution of autumn phenology to changes in
302 satellite-derived growing season length estimates across Europe (1982–2011). Global
303 Change Biology, 20, 3457-3470.

304 20. Yang, Y., et al (2015). Changes in autumn vegetation dormancy onset date and the
305 climate controls across temperate ecosystems in China from 1982 to 2010. Global change
306 biology, 21, 652-665.
307 21. Jeong, S. J., et al (2011). Phenology shifts at start vs. end of growing season in
308 temperate vegetation over the Northern Hemisphere for the period 1982–2008. Global
309 Change Biology, 17, 2385-2399.
310 22. Peng, S., et al (2013). Asymmetric effects of daytime and night-time warming on
311 Northern Hemisphere vegetation. Nature, 501, 88-92.
312 23. Beguería, S., et al (2014). Standardized precipitation evapotranspiration index (SPEI)
313 revisited: parameter fitting, evapotranspiration models, tools, datasets and drought
314 monitoring. International Journal of Climatology, 34, 3001-3023.
315 24. Meng, T.T, et al (2009). Plant morphometric traits and climate gradients in northern
316 China: a meta-analysis using quadrat and flora data. Annals of Botany, 104,1217-1229.
317 25. Prasad, V.K., et al. (2007). Spatial patterns of vegetation phenology metrics and
318 related climatic controls of eight contrasting forest types in India - analysis from remote
319 sensing datasets. Theoretical and Applied Climatology, 89:95-107
320 26. Peñuelas J., et al. (2013). Evidence of current impact of climate change on life: a walk
321 from genes to the biosphere. Global Change Biology,19, 2303-2338.
322 27. Wolf, A.A., et al. (2017). Flowering phenology shifts in response to biodiversity
323 loss. Proceedings of the National Academy of Sciences, 114, 3463-3468.
324 28. Fu, Y. S., et al (2014). Variation in leaf flushing date influences autumnal senescence
325 and next year's flushing date in two temperate tree species. Proceedings of the National

Academy of Sciences, 111, 7355-7360.

29. Wolf, S., et al (2016). Warm spring reduced carbon cycle impact of the 2012 US summer drought. Proceedings of the National Academy of Sciences, 113, 5880-5885.

30. Peñuelas, J., et al (2017). Shifting from a fertilization-dominated to a warming-dominated period. Nature Ecology & Evolution, 1, 1438-1445.

Methods

1. Phenological observation data

We used observations of leaf senescence date (LSD) from three independent phenological datasets.

1) The Pan European Phenological Database (PEP725; http://www.pep725.eu/), an open-access database with long term plant phenological observations (since 1868) from 19608 sites and 78 species across 25 European countries.

2) The China Phenological Observation Network (CPON), with data since 1963 for >100 species at 42 sites across China.

3) LSD data for two tree species (*Acer palmatum* and *Ginkgo biloba*) at 54 meteorological stations in South Korea for 1989-2007[31].

The definitions of LSD notably differ among the datasets. LSD for the PEP725, CPON, and Korean datasets is defined as the date when 50, 90, and 20% of the tree leaves, respectively, change color from green to red or yellow. We removed outliers using the methods[32] to exclude potential biases and inadequate degrees of freedom and focused on time series with at least 15 years of records for1900-2015. We thus analyzed 14536 LSD

time series for 24 species (Table S1).

2. LSD derived from satellite data

LSD in the Northern Hemisphere was determined using two satellite-derived vegetation indices, the Normalized Difference Vegetation Index (NDVI) and the Enhanced Vegetation Index (EVI)[33]. Both NDVI and EVI are direct indictors of vegetation growth and have been widely applied for investigating vegetation phenology[34]. We used two datasets to reduce the uncertainties caused by a single data source: GIMMS NDVI third-generation (NDVI3g) data derived from the Advanced Very High Resolution Radiometer (AVHRR) and NDVI and EVI derived from the Moderate Resolution Imaging Spectroradiometer (MODIS). The GIMMS NDVI3g data have a spatial resolution of 1/12°, a half-month interval, and a 34-year time span (1982-2015). The MODIS 16-day composite product MOD13C1 (Collection 6) includes both NDVI and EVI with a 0.05° resolution for 2001-2015.

We eliminated the impacts of areas with sparse vegetation on the results by first excluding pixels with annual NDVI <0.1 or annual EVI <0.08[35]. A Savitzky-Golay filter was then used to smooth the NDVI (EVI) time series[36]. We then estimated LSD using two methods.

The first method was a dynamic-threshold approach, which uses an annually defined threshold for each pixel based on the NDVI ratio:

$$NDVI_{ratio} = (NDVI - NDVI_{\min}) / (NDVI_{\max} - NDVI_{\min}) \quad (1)$$

where NDVI is the daily NDVI and $NDVI_{max}$ and $NDVI_{min}$ are the annual daily maximum

and minimum of NDVIs. The $NDVI_{ratio}$ ranges from 0 to 1. LSD is determined when $NDVI_{ratio}$ decreases to 0.5 in autumn[37,38].

The second method was based on a series of piecewise logistic functions. The NDVI time series were first divided into two sections by the maximum daily NDVI in each year, and a double logistic function was applied to fit each section[39]:

$$y(t) = a_1 + (a_2 - a_7 t)\left[\frac{1}{1 + e^{(a_3 - t)/a_4}} - \frac{1}{1 + e^{(a_5 - t)/a_6}}\right] \quad (2)$$

LSD was then defined as the time when the curvature changing rate reached its last local maximum value.

For GIMMS3g data, we calculated LSD using NDVI from both the dynamic-threshold approach and the piecewise logistic function method. Since MODIS sensor provides EVI, we further used EVI-based logistic function method to derive LSD. To sum up, for GIMMS3g data, average LSD from threshold and logistic function method were used, and for MODIS, an additional LSD from EVI-based logistic function method was used (not for MODIS NDVI data).

At high latitudes (or elevations), snow cover is important for regional climate and arrives early in autumn and potentially masking evergreen vegetation. However, we suggested that using a Savitzky-Golay filter could solve the noise from a "sudden" change in the time series of NDVI due to snow[36]. In particular, a study showed that snowfall had little influence on determining EOS in western Arctic Russia[41]. For high elevations, our previous analysis on Tibetan Plateau showed that for more than 98% of regions snow happened later than LSD[42].

3. Climatic data

We used the CRU-TS 4.00 dataset with a spatial resolution of 0.5°×0.5° for 1901-2015. We extracted monthly data for T_{max}, T_{min}, T_{mean}, precipitation, and cloud cover from this dataset for analyzing LSD from in-situ observations and the two remote sensing data. We modeled past and future LSD by temperature by acquiring daily gridded data for maximum and minimum temperature with a spatial resolution of 0.5° from NOAA Earth System Research Laboratory Physical Sciences Division for 1982-2015. We used daily T_{max} and T_{min} simulated by the CCSM 4 model under two climatic scenarios (RCP4.5 and RCP8.5) for future climatic data (2081-2100). These data were from an open-access database of the Coupled Model Intercomparison Project Phase 5.

4. Analyses

We used partial correlation analyses to determine the responses of LSD to T_{day} and T_{night}. The reason is that directly correlating LSD to T_{day} would give misleading results since T_{night} is a confounding variable that is numerically related to both LSD and T_{day}, violating independence of variables in multiple correlation tests. Thus, using the partial correlation between LSD and T_{day} will measure the degree of association with the effect of a set of controlling random variables removed (e.g., T_{night}, precipitation, radiation), given that these factors have shown strong influences on LSD[10, 20]. Since Echer and Silva (2014) demonstrated that clouds are the main atmospheric factor modulating the surface incidence of solar radiation[43], cloud cover data was used to model the effect of radiation on LSD, as similarly conducted in previous analyses[8]. Correlations were classified into

four types, (A) $T_{day}^{+}T_{night}^{+}$, (B) $T_{day}^{-}T_{night}^{-}$, (C) $T_{day}^{+}T_{night}^{-}$ and (D) $T_{day}^{-}T_{night}^{+}$, where T^{+}, T^{-} represent positive and negative partial correlation coefficient of T with LSD. An R of at least 0.514 for MODIS is required for the significance test ($p = 0.05$), but this value decreases to 0.339 for the longer GIMMS3g data. These analyses were investigated for both Köppen-Geiger climatic classifications and vegetation types (Table S2[40]). Crops were excluded because their signal may result from changes in cropping or harvest cycles, rather than from climate change. Furthermore, since at low latitudes plant phenology of tropical and subtropical areas responds to other factors than temperature, regions with latitudes < 20° N were also excluded.

Current phenology algorithms in most terrestrial-biosphere models are solely based on temperatures in the preceding months[44-45]. We determined the length of the preseason whose average T_{day} had the most influence on LSD by calculating the partial correlation coefficients between LSD and mean T_{day} during 0, 1, 2, … *n* months prior to LSD, controlling for corresponding mean T_{night}, total precipitation, and radiation. The maximum range (*n*) of the preseason is generally from June to the multiyear mean date of LSD (see Fig. S20 for example). The partial correlation coefficients with the highest absolute values were then used in the following analysis. We obtained the relationship between LSD and T_{night} the same way but replacing T_{day} with T_{night}. This analytical procedure was applied for observed LSD from ground sites and derived LSD from the MODIS and GIMMS NDVI3g data.

5. Models for predicting LSD

Our results indicated that LSD responded oppositely to T_{day} and T_{night}, so we developed a weighted day-night-temperature growing-degree-day (DN_{GDD}) algorithm from observations to model LSD, and compared the algorithm with currently used threshold and GDD models based on T_{mean}[46].

The threshold model was the simplest method. We calculated average T_{mean} for five days before LSD in each year and used the multiyear mean value as the threshold to model LSD. If T_{mean} was lower than the threshold for five consecutive days from 1st July, the last date was considered the LSD.

GDD was calculated as:

$$GDD(d) = \max(T_b - T_{mean}(d), 0) \quad (3)$$

$$GDD_{threshold} = \sum_{d=d_0}^{LCD} GDD(d) \quad (4)$$

where T_b is the base temperature set to 15, 20, 25, and 30 °C, $T_{mean}(d)$ is the mean daily temperature, and d_0 is the date on which the calculation begins (1st July in this study). LSD is the observed or derived date of leaf coloring in each year. The date when $GDD(d)$ exceeded the multiyear average GDD threshold was defined as LSD.

Our DN_{GDD} model improved upon the original GDD model and was calculated by:

$$GDD(d) = k \cdot \max(T_b - T_{day}(d), 0) + (1 - k) \cdot \max(T_b - T_{night}(d), 0) \quad (5)$$

where $T_{day}(d)$ is the daily maximum temperature, $T_{night}(d)$ is the daily minimum temperature, and k is the weighting factor. When $0<k<1$, the effects of T_{day} and T_{night} on LSD are consistently positive; When $k>1$ or $k<0$, the effects of T_{day} and T_{night} on LSD are opposite. In order to determine the value of k, we first calculated the ratio of R_{day} and R_{night} for each station or pixel, and found 99.9% of the ratio values were between -10 and 10 for

458 both ground and satellite data (Figure S21). In other words, the level of T_{day}(T_{night}) effect
459 could be 1 to 10 times than the level of T_{night}(T_{day}) effect (note that T_{day} represents T_{day} with
460 the effects of T_{night} removed). Therefore, the values of k ranged from –1 to 2 (see Table
461 S3). In addition, when k tends to infinity, the effects of T_{day} and T_{night} on LSD are opposite
462 with same level.

463 We evaluated the accuracy and obtained the most appropriate parameters of the
464 models by calculating the correlation coefficient (R) and the root mean square error
465 (RMSE) between modeled and observed LSD. T_b and k with the lowest RMSE were
466 considered the most appropriate values for each site or pixel.

467

468 **Data Availability**

469 The data that support the findings of this study are available from the corresponding
470 author upon request.

471

472 **References**

473 31. Park, C.K., et al., (2017). Spatial and temporal changes in leaf coloring date of Acer
474 palmatum and Ginkgo biloba in response to temperature increases in South Korea.
475 PLoS ONE, 12.
476 32. Schaber, J., & Badeck, F.W. (2002). Evaluation of methods for the combination of
477 phenological time series and outlier detection. Tree Physiology, 22, 973-982.
478 33. Huete, A., et al., (2002). Overview of the radiometric and biophysical performance of
479 the MODIS vegetation indices. Remote sensing of environment, 83, 195-213.

480 34. Zhang, X., et al. (2003). Monitoring vegetation phenology using MODIS. Remote
481 sensing of environment, 84, 471-475.
482 35. Shen, M., et al., (2014). Increasing altitudinal gradient of spring vegetation phenology
483 during the last decade on the Qinghai–Tibetan Plateau. Agricultural and Forest
484 Meteorology, 189, 71-80.
485 36. Chen, J., et al., (2004). A simple method for reconstructing a high-quality NDVI
486 time-series data set based on the Savitzky–Golay filter. Remote sensing of
487 environment, 91, 332-344.
488 37. Piao, S., et al., (2011). Changes in satellite-derived vegetation growth trend in
489 temperate and boreal Eurasia from 1982 to 2006. Global Change Biology, 17,
490 3228-3239.
491 38. White, M.A., et al. (1997). A continental phenology model for monitoring vegetation
492 responses to interannual climatic variability. Global Biogeochemical Cycles, 11,
493 217-234.
494 39. Elmore, A.J., et al., (2012). Landscape controls on the timing of spring, autumn, and
495 growing season length in mid-Atlantic forests. Global Change Biology, 18,
496 656-674.
497 40. Olson, D. M., et al. (2001). Terrestrial ecoregions of the world: a new map of life on
498 earth. Bioscience, 51, 933-938.
499 41. Zeng, H., & Jia, G. (2013). Impacts of snow cover on vegetation phenology in the
500 arctic from satellite data. Advances in Atmospheric Sciences, 30, 1421-1432.
501 42. Wang, X. et al. 2018. Snow cover phenology affects alpine vegetation growth

502 dynamics on the Tibetan Plateau: Satellite observed evidence, impacts of biomes,
503 and climate drivers. Agricultural and Forest Meteorology, 256, 61-74.
504 43. Silva, A. A., & Echer, M. P. D. S. (2013). Ground-based measurements of local cloud
505 cover. Meteorology & Atmospheric Physics, 120, 201-212.
506 44. Delpierre, N., et al. (2009). Modelling interannual and spatial variability of leaf
507 senescence for three deciduous tree species in france. Agricultural & Forest
508 Meteorology,149, 938-948.
509 45. Richardson, A.D., et al., (2012). Terrestrial biosphere models need better
510 representation of vegetation phenology: results from the North American Carbon
511 Program Site Synthesis. Global Change Biology, 18, 566-584.
512 46. Krinner, G., et al., (2005). A dynamic global vegetation model for studies of the
513 coupled atmosphere-biosphere system. Global Biogeochemical Cycles, 19,
514 doi:10.1029/2003GB002199.

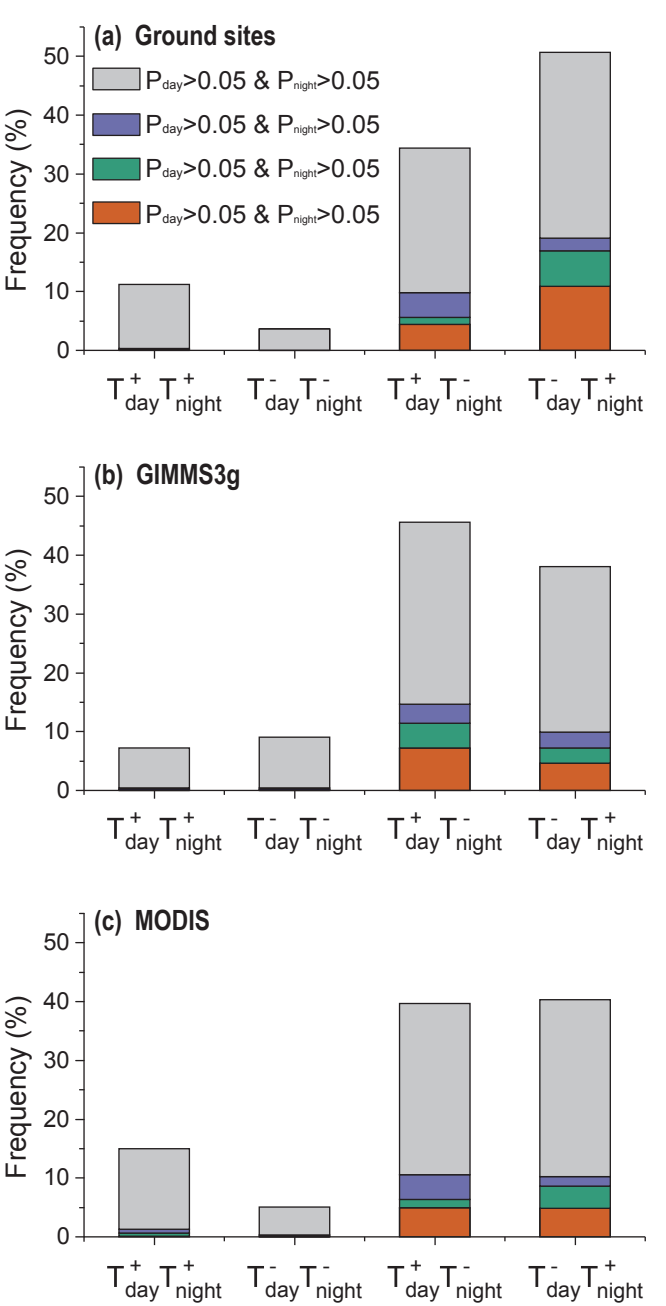
(a) Ground sites
P_{day}>0.05 & P_{night}>0.05
P_{day}>0.05 & P_{night}>0.05
P_{day}>0.05 & P_{night}>0.05
P_{day}>0.05 & P_{night}>0.05
Frequency (%)
0
10
20
30
40
50
$T^{+}_{day}T^{+}_{night}$
$T^{-}_{day}T^{-}_{night}$
$T^{+}_{day}T^{-}_{night}$
$T^{-}_{day}T^{+}_{night}$
(b) GIMMS3g
Frequency (%)
0
10
20
30
40
50
$T^{+}_{day}T^{+}_{night}$
$T^{-}_{day}T^{-}_{night}$
$T^{+}_{day}T^{-}_{night}$
$T^{-}_{day}T^{+}_{night}$
(c) MODIS
Frequency (%)
0
10
20
30
40
50
$T^{+}_{day}T^{+}_{night}$
$T^{-}_{day}T^{-}_{night}$
$T^{+}_{day}T^{-}_{night}$
$T^{-}_{day}T^{+}_{night}$

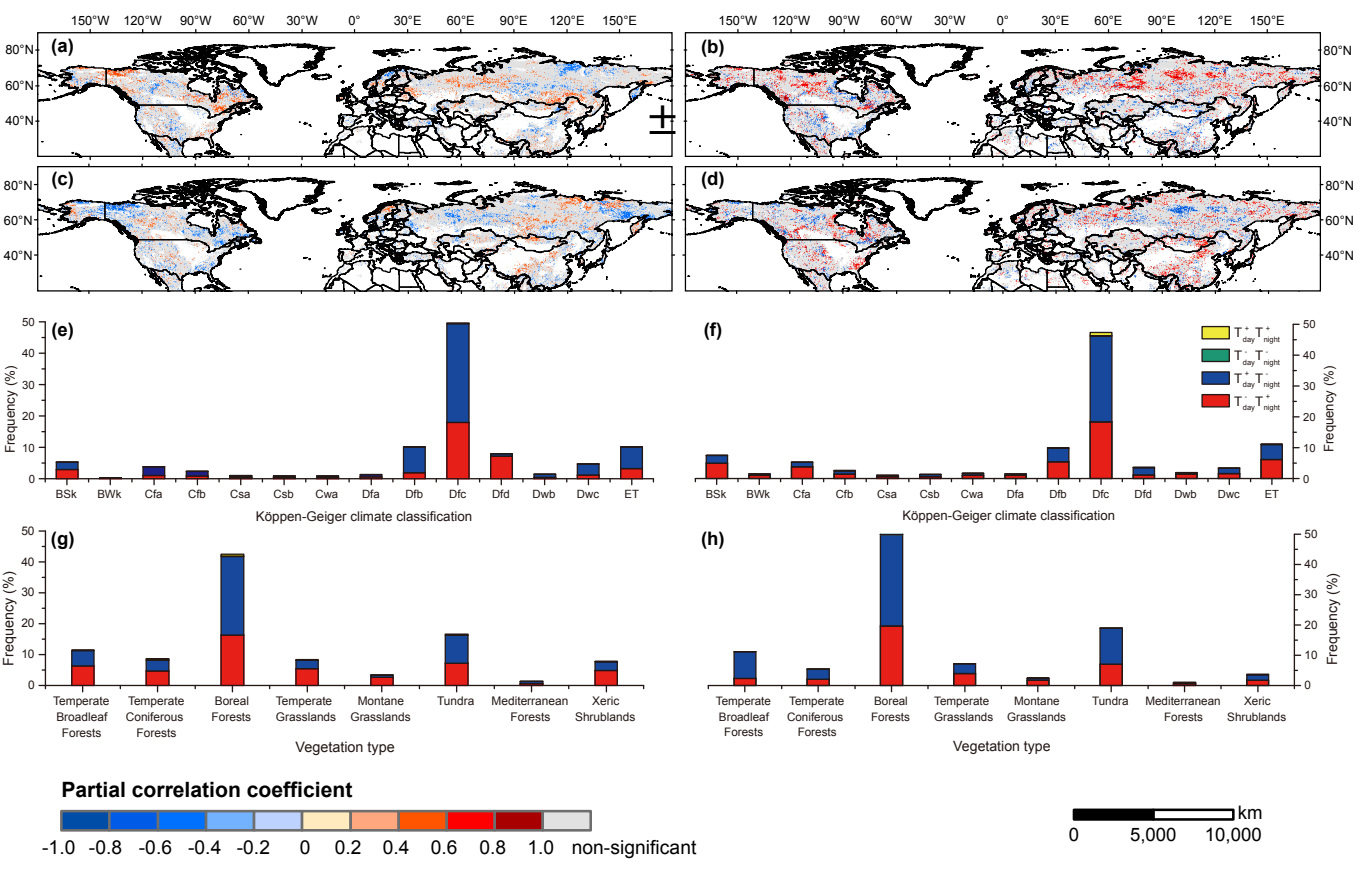
(a)
(b)
(c)
(d)
150°W 120°W 90°W 60°W 30°W 0° 30°E 60°E 90°E 120°E 150°E
80°N
60°N
40°N
(e)
(f)
Frequency (%)
BSk BWk Cfa Cfb Csa Csb Cwa Dfa Dfb Dfc Dfd Dwb Dwc ET
Köppen-Geiger climate classification
$T^+_{day}T^+_{night}$
$T^+_{day}T^-_{night}$
$T^-_{day}T^-_{night}$
$T^-_{day}T^+_{night}$
(g)
(h)
Temperate Broadleaf Forests
Temperate Coniferous Forests
Boreal Forests
Temperate Grasslands
Montane Grasslands
Tundra
Mediterranean Forests
Xeric Shrublands
Vegetation type
Partial correlation coefficient
-1.0 -0.8 -0.6 -0.4 -0.2 0 0.2 0.4 0.6 0.8 1.0 non-significant
km
0 5,000 10,000

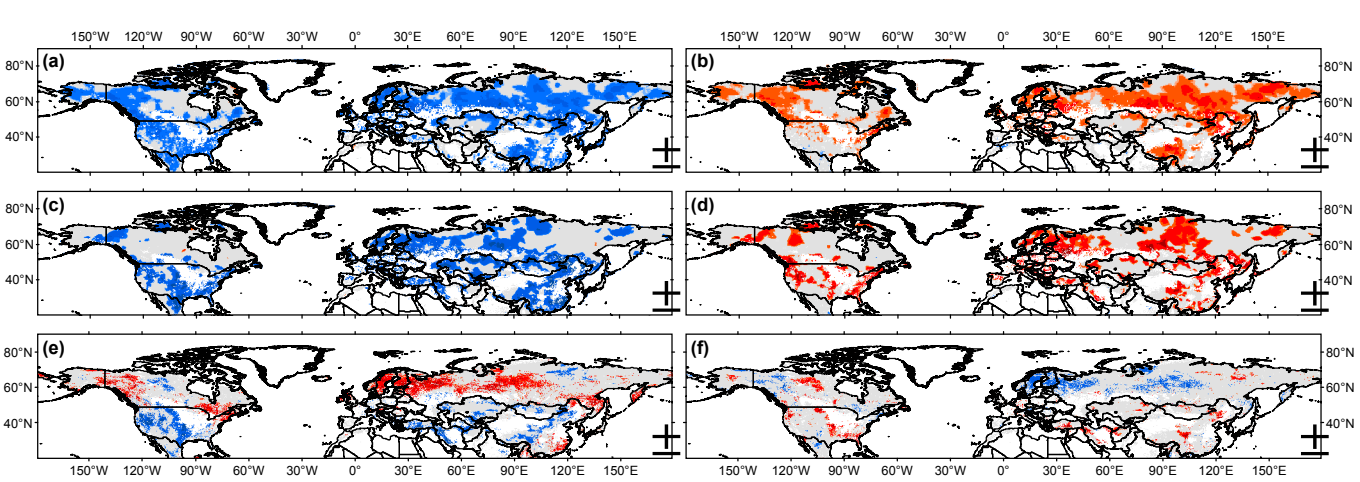
(a)
(b)
(c)
(d)
(e)
(f)
150°W 120°W 90°W 60°W 30°W 0° 30°E 60°E 90°E 120°E 150°E
80°N
60°N
40°N
Partial correlation coefficient
-1.0 -0.8 -0.6 -0.4 -0.2 0 0.2 0.4 0.6 0.8 1.0 non-significant
km
0 5,000 10,000

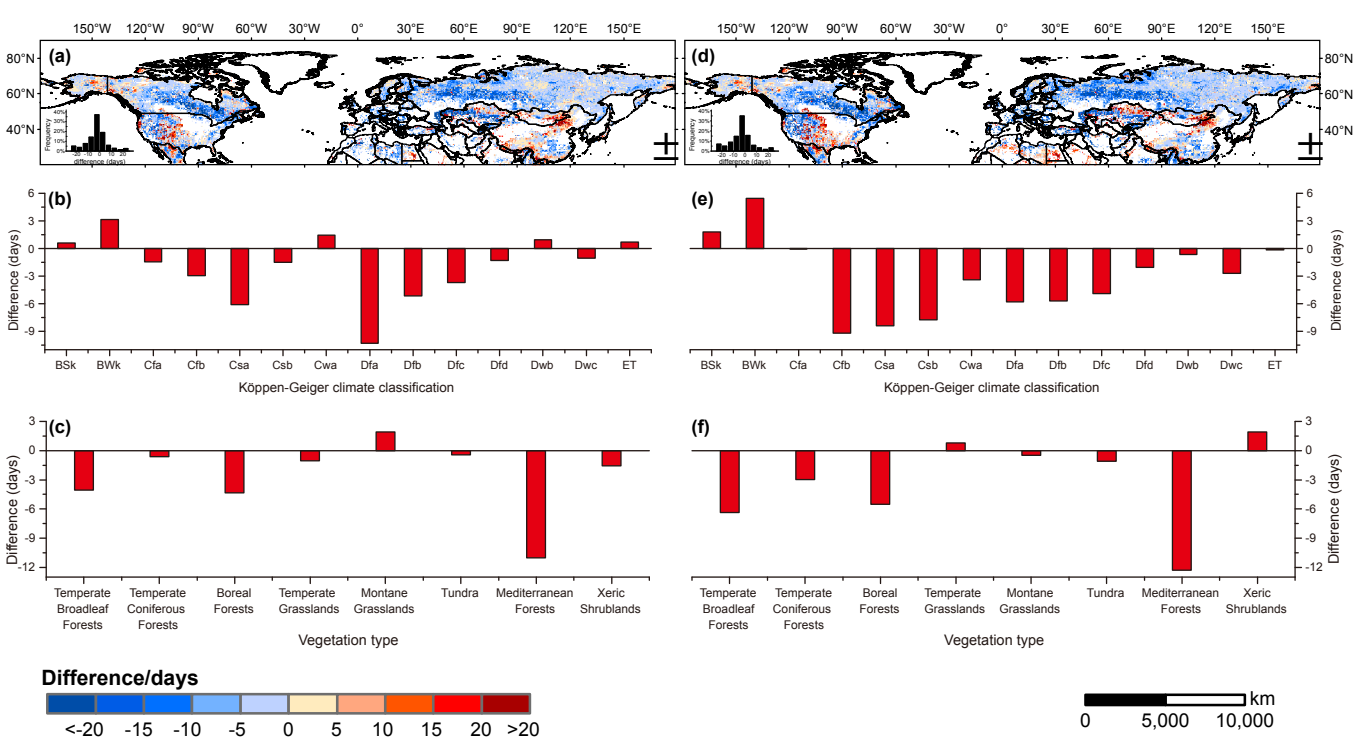
(a)
(b)
(c)
(d)
(e)
(f)
150°W 120°W 90°W 60°W 30°W 0° 30°E 60°E 90°E 120°E 150°E
80°N
60°N
40°N
Frequency
difference (days)
Difference (days)
BSk BWk Cfa Cfb Csa Csb Cwa Dfa Dfb Dfc Dfd Dwb Dwc ET
Köppen-Geiger climate classification
Temperate Broadleaf Forests
Temperate Coniferous Forests
Boreal Forests
Temperate Grasslands
Montane Grasslands
Tundra
Mediterranean Forests
Xeric Shrublands
Vegetation type
Difference/days
<-20 -15 -10 -5 0 5 10 15 20 >20
km
0 5,000 10,000